Geomorphology xxx (2014) xxx–xxx

Contents lists available at ScienceDirect

Geomorphology

journal homepage: www.elsevier.com/locate/geomorph

The tectonic geomorphology of bedrock scarps on active normal faults in the Italian Apennines mapped using combined ground penetrating radar and terrestrial laser scanning

A. Bubeck [g,1], M. Wilkinson [a], G.P. Roberts [c], P.A. Cowie [e], K.J.W. McCaffrey [b], R. Phillips [d], P. Sammonds [f]

[a] Geospatial Research Ltd., Department of Earth Sciences, Durham University, Durham, UK
[b] Department of Earth Sciences, Durham University, Durham, UK
[c] Department of Earth and Planetary Sciences, Birkbeck, University of London, London, UK
[d] School of Earth and Environment, University of Leeds, Leeds, UK
[e] University of Bergen, Department of Earth Science, P.O. Box 7803, N-5020 Bergen, Norway
[f] Institute for Risk and Disaster Reduction, University College London, London, UK
[g] School of Earth and Ocean Sciences, Cardiff University, Cardiff, Wales, UK

ARTICLE INFO

Article history:
Received 24 July 2012
Received in revised form 4 October 2013
Accepted 4 March 2014
Available online xxxx

Keywords:
Apennines
Bedrock fault scarps
Paleoseismology
LiDAR
GPR

ABSTRACT

Using combined datasets from ground penetrating radar (GPR) and terrestrial laser scanning (TLS) we document the variety of tectono-geomorphic features that contribute to the morphology of bedrock scarps associated with active extensional faulting in central Italy. Measurement of faulted offsets across such scarps can provide important fault slip-rate data relevant to seismic hazard analysis if ages can be established for offset features. However, interpretation of these offsets is challenging when geomorphic processes as well as fault slip contribute to exhumation of the bedrock during scarp development. Through the integration of surface (TLS) and subsurface (GPR) datasets, we show that the surface expression of three bedrock scarps results from the interaction between footwall incision, hangingwall sedimentation, channel incision and landsliding as well as fault slip and fault linkage. We further illustrate how these processes can be differentiated to identify locations suitable for determining fault slip-rates. The identification of such features has important implications for our understanding of the relationship between bedrock faulting and geomorphic processes, in turn contributing to improved assessment of fault slip-rates in the central Apennines. The use of combined GPR and TLS datasets here has shown that the tectono-geomorphic features of the studied scarps vary greatly over short distances and we emphasise the need for detailed scarp analysis to elucidate the processes responsible for bedrock exhumation before estimating the rates of fault slip over the timescale of scarp formation.

1. Introduction

Bedrock fault scarps form prominent features in the landscape of the central Apennines of Italy where active extensional deformation is associated with devastating earthquakes (Bosi et al., 1993; Piccardi et al., 1999; Roberts and Michetti, 2004; Faure Walker et al., 2010; e.g. 1915 Ms 6.9 Avezzano earthquake, 33,000 deaths). These fault scarps are a key archive of both the fault slip responsible for earthquakes in the Holocene and the geomorphic response to climatic change following the demise of the last glacial maximum. This paper presents new data collected from combined ground penetrating radar (GPR) and LiDAR studies (terrestrial laser scanning — TLS) that allow us to recognise key elements of the geometry of these faults scarps that we can use to study earthquake slip and the geomorphic response to climatic change.

The formation and preservation of fault scarps in the landscape of central Italy is a direct consequence of a change in surface processes and rates that occurred at 15 ± 3 ka, when erosion and sedimentation rates decreased after the demise of the last glacial maximum (Allen et al., 1999; Roberts, 2006; Faure Walker et al., 2010; Tucker et al., 2011). For one active fault, the erosion rate perpendicular to the slope on carbonate bedrock was ~0.2–0.4 mm/yr prior to the Holocene, decreasing to 0.016 ± 0.005 mm/yr as the climate changed after the demise of the last glacial maximum, constrained by measurements of fault plane degradation; the throw-rate (vertical component of the slip-rate) across the fault was 1 ± 0.07 mm/yr measured in this latter period (Tucker et al., 2011 and results shown below). Thus, during the last glacial maximum, rates of repeated surface fault slip during earthquakes driven by regional tectonics were approached or outpaced by rates of freeze/thaw-driven footwall erosion, leading to degradation and in places removal and/or sedimentary burial of the fault scarps (Roberts and Michetti, 2004; Tucker et al., 2011). Following the last glacial

[1] Current affiliation: School of Earth and Ocean Sciences, Cardiff University, UK.

http://dx.doi.org/10.1016/j.geomorph.2014.03.011

maximum, the rate of erosion and sedimentation declined and renewed growth of vegetation stabilised mountain slopes. The combination of lower rates of erosion and continued fault movement associated with earthquakes led to the formation of bedrock fault scarps, commonly with "free-face" fault planes composed of Mesozoic limestones. Post-glacial tectonic displacement of the periglacial surfaces and glaciogenic deposits across the fault scarps has been used to conclude on Holocene fault slip-rates (Piccardi et al., 1999; Galadini and Galli, 2000; Roberts and Michetti, 2004; Papanikolaou et al., 2005; Faure Walker et al., 2009, 2010; Reicherter et al., 2011). Rates of throw accumulation measured in this way lie in the range of ~0.2–1.3 mm/yr because measured vertical offsets across scarps are in the range 3–20 m. These throw-rate estimates have been used in geomorphic studies to investigate the style and rate of landscape response to tectonic forcing (e.g. Whittaker et al., 2007a,b, 2008; Attal et al., 2008, 2011; Cowie et al., 2008). The combination of these data with paleoseismic trench studies and historical records places constraints on earthquake recurrence intervals and evaluation of the seismic hazard posed by major faults (Roberts et al., 2004). In particular, throw-rates derived from offsets across bedrock scarps help constrain rates of earthquake recurrence averaged over multiple earthquake cycles. For example, paleoseismic trench studies in Italy have recorded a maximum of 5 earthquakes at a given site (Pantosti et al., 2003), but more typically include 1–3 earthquakes that are restricted to the last c. 5000 years (see Galli et al., 2008 for a review). These data provide important constraints of the magnitude of past earthquakes and the approximate timing of rupture. However, with earthquake recurrence intervals measured from paleoseismological trenches, ranging from ~500 to ~10,000 years (see Faure Walker et al., 2010 for a review) it is unlikely that all seismic sources will have been activated during the historical record, which is probably reliable for earthquakes of magnitude ~ >M 6.0 since 1349 A.D. (Roberts and Michetti, 2004), or even the paleoseismic record recoverable from traditional trench site investigations (~5000 years). A record longer than both the historical record and the paleoseismic record from traditional trenching will be required to quantify recurrence intervals, and in particular temporal clustering of earthquakes. In fact, studies of synthetic seismicity datasets have shown that a time period that is at least ~6 times the length of the average earthquake recurrence interval is needed to capture the key elements of slip-rate variability produced by temporal earthquake clustering (see Cowie et al., 2012). The study of slip across fault scarps, thought to have formed since the last glacial maximum at 15 ± 3 ka (Roberts and Michetti, 2004; Faure Walker et al., 2010) may be the only pragmatic way to gain such a record.

Recently *in situ* ^{36}Cl cosmogenic exposure dating of bedrock fault scarps has shown the potential for this method to derive records of earthquake slip that encompass multiple seismic cycles (e.g. Benedetti et al., 2002; Palumbo et al., 2004; Schlagenhauf et al., 2010, 2011). However, in this paper we suggest that the required analysis of the relative extent of tectonic and geomorphic exhumation mechanisms for such bedrock faults scarps is, in practice, very challenging without a subsurface constraint from shallow geophysics and high resolution DEMs of the scarps. The correct interpretation of subtle features in the landscape, such as landslides, colluvial wedges, and incision of the footwall and hangingwall by slope and fluvial processes can lead to contrasting conclusions on the amount of slip-related exhumation that exists; recognition and correct interpretation of such geomorphic features is essential to choose sites for *in situ* ^{36}Cl cosmogenic exposure dating of bedrock fault scarps. To reduce such ambiguity, we describe 3 fault scarp locations that we have studied using a combination of terrestrial LiDAR to produce high resolution DEMs and ground penetrating radar, allowing us to review the types of observations that must be made to differentiate exhumation of fault planes by tectonic slip and by exhumation/burial resulting from erosion, landsliding or sedimentation.

The Fiamignano, Tre Monti and Magnola faults (Fig. 1) investigated in this study belong to the central Apennines fault array. Exhumation of these fault scarps and their associated fault planes has been previously interpreted to have been produced either solely by fault slip or through concomitant erosion/sedimentation and landsliding (Bosi et al., 1993). We attempt to review and refine the findings of previous work using a combination of ground penetrating radar (GPR) surveys and terrestrial laser scanning (TLS) datasets and provide a method from which the surface to subsurface characteristics of bedrock fault scarps and the spatial extent of relevant scarp-forming processes can be characterised with high spatial resolution.

2. Geological background

The Apennine Mountain chain is a narrow NW–SE oriented thrust belt belonging to the Alpine orogenic system, with superimposed Quaternary extensional faulting. Contemporaneous migration of a compressive front in the late-Cretaceous and Mio-Pliocene with subduction to the east and the opening of the Tyrrhenian Sea to the west resulted in the early stages of formation of the mountain chain (Patacca et al., 1990). Gradual migration of crustal shortening and thickening in the NE and E directions was followed by active extension during the Quaternary, resulting in the formation of a complex array of NW–SE trending normal faults (Anderson and Jackson, 1987; Fig. 1). D'Agostino et al. (2001) argue that the extension is the response to uplift driven by mantle upwelling beneath the central Apennines and that this has been the dominant geodynamical process during the Quaternary (see also Faure Walker et al., 2012). Regardless of the underlying mechanism the present day tectonic activity in this area is dominated by normal faulting earthquakes along NW–SE trending fault planes. The prominent Holocene bedrock fault scarps have been used to quantify the long term rate of extension across the region (Holocene averaged rate: 3.1 ± 0.7 mm/yr; Faure Walker et al., 2012) and this is broadly consistent with estimates from geodesy (e.g. Serpelloni et al., 2005; D'Agostino et al., 2011).

Previous studies have identified and reviewed the important paleoseismological significance of bedrock fault scarps in constraining the locations, magnitudes and recurrence intervals for large earthquakes in the central Apennines (see Stewart and Hancock, 1990; Bosi et al., 1993; Giaccio et al., 2002; Palumbo et al., 2004; Michetti et al., 2005; Papanikolaou et al., 2005; Schlagenhauf, 2009; Schlagenhauf et al., 2010). Propagation of fault slip to the surface along bedrock scarps has been observed in both the 1915 Avezzano earthquake (Ms 6.9–7.0, 33,000 deaths, Michetti et al., 1996; Salvi et al., 2003; c. 1 m surface slip), and the 1980 Irpinia earthquake (Ms 6.9, 3000 deaths, Westaway and Jackson, 1984; also c. 1 m surface slip). Even the 2009 L'Aquila earthquake (Mw 6.3, 308 deaths, Walters et al., 2009) with the majority of its ruptures found within Quaternary/Holocene deposits, exhibits locations where slip has migrated to the surface along bedrock fault scarps (Boncio et al., 2010). The advent of ^{36}Cl *in situ* cosmogenic dating of emergent fault planes has yielded important records of the magnitude and ages of paleoearthquakes, with the timing of slip constraining recurrence intervals, dating back 7–12 kyr (Palumbo et al., 2004; Schlagenhauf et al., 2010, 2011). At one site on the Magnola Fault in central Italy, it is suggested as many as 5 paleoearthquakes have taken place in the last 7200 years (7.2 ka, 4.9 ka, 4.0 ka, 3.4 ka and 1.5 ka; Schlagenhauf et al., 2010, see also Palumbo et al., 2004), opening the way for the study of other sites, which may provide a greater record of older and more numerous events. However, Bosi et al. (1993) and Giaccio et al. (2002), caution that the definition of the number of displacement events and their occurrence age may only be obtained through the study of emergent fault planes if non-tectonic means of exhuming/burying bedrock fault scarps are considered and steps are taken to avoid studying at sites where erosion, sedimentation and landsliding may be responsible for scarp exhumation. This paper attempts to quantify the roles of tectonic fault slip in earthquakes, as opposed to erosion, sedimentation and landsliding in exhuming carbonate fault planes associated with bedrock fault scarps. We do this through study of 3 sites along active

Please cite this article as: Bubeck, A., et al., The tectonic geomorphology of bedrock scarps on active normal faults in the Italian Apennines mapped using combined ground penetrating..., Geomorphology (2014), http://dx.doi.org/10.1016/j.geomorph.2014.03.011

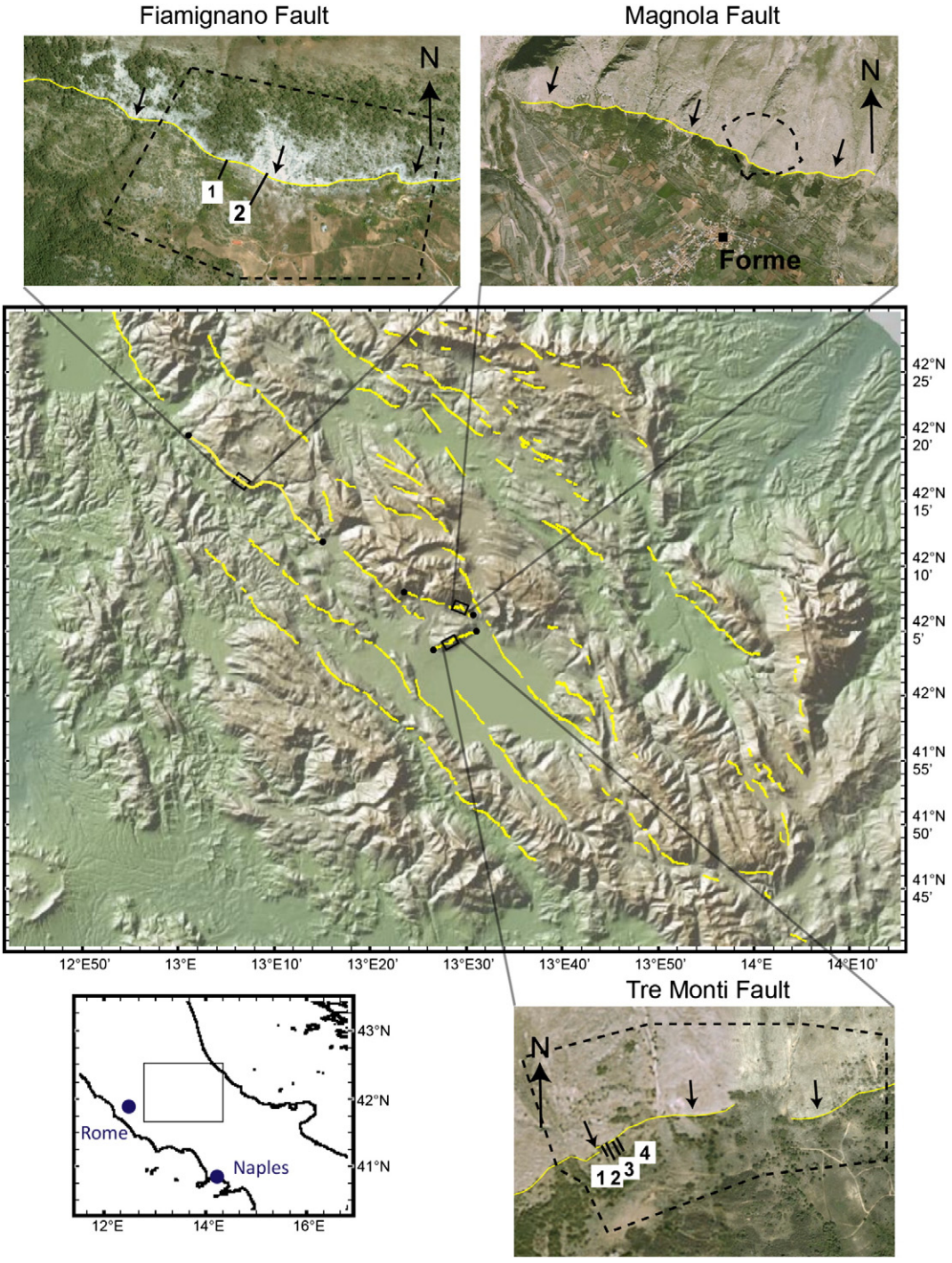

Fig. 1. The location and extent of the study area and surveys along the three faults used in this study within the overall Apennine fault array. Black circles at the end of each fault represent the fault tips. The inset maps for Fiamignano, Magnola and Tre Monti show the active fault trace (solid lines), TLS data extent (black dashed line) and the GPR transect lines (numbered black lines).
Imagery from Google Earth™.

faults: the Magnola Fault; the Fiamignano Fault; and the Tre Monti Fault.

2.1. The Magnola Fault

The Magnola Fault (Fig. 1) is a WNW–ESE striking normal fault, sampled in the ^{36}Cl studies of Palumbo et al. (2004) and Schlagenhauf et al. (2010). Recent Quaternary activity is manifested by the existence of a c. 5–15 m high bedrock fault scarp and the presence of geomorphic features including triangular facets and perched valleys (Palumbo et al., 2004). The fault scarp places fractured and grain-size reduced Mesozoic limestones against Quaternary/Holocene sediments, and offsets a land surface, widely-believed to date from the last glacial maximum, vertically by ~15 m. A study of erosion at this site by Tucker et al. (2011) notes high erosion rates during the last glaciation (0.22–0.28 mm/yr quasi-perpendicular to the periglacial footwall slope), and a reduction in this rate after the glacial maximum (to 0.016 ± 0.005 mm/yr, quasi-perpendicular to the fault plane) allowing the

Please cite this article as: Bubeck, A., et al., The tectonic geomorphology of bedrock scarps on active normal faults in the Italian Apennines mapped using combined ground penetrating..., Geomorphology (2014), http://dx.doi.org/10.1016/j.geomorph.2014.03.011

preservation of Holocene bedrock scarps. Previous paleoseismological studies on this fault yield slip rates of 0.8 ± 0.1 mm/yr from concentrations of in situ cosmogenic ^{36}Cl that has accumulated on a well preserved section of the 10 km long fault scarp over the last 7–12 kyr (Palumbo et al., 2004; Schlagenhauf et al., 2010; the latter paper extends and re-analyses the former, supporting the 7 rather than 12 ka age) with earthquake events suggested at 7.2 ka, 4.9 ka, 4.0 ka, 3.4 ka and 1.5 ka. Carcaillet et al. (2008), studying chemical variations of the fault plane, identified soil signatures within the carbonate fault rocks at heights on the fault plane that appear to correlate with the paleoground surfaces identified with ^{36}Cl dating by Palumbo et al., 2004 (and hence Schlagenhauf et al., 2010). These chemical variations occur in areas where the fault plane paused in the zone of active soil formation for long periods of quiescence between slip increments, and can be correlated with the ^{36}Cl dating. Comparable slip rates were obtained by Piccardi et al. (1999) who used geomorphic offsets to derive slip rates of 0.7 ± 0.3 mm/yr for this fault. Slip per earthquake on this fault has been discussed by Schlagenhauf et al. (2011). The dimensions of so-called "cusps" in the ^{36}Cl versus elevation on the fault plane data suggest 2–4 m sized slip events and this is consistent with the 2–4 m spacing of chemical banding on the fault plane (Carcaillet et al., 2008). However, 2–4 m slip events would be very unusual on this fault as its length is only ~10 km. If the slip events adhere to the scaling relationships for global studies of earthquakes (Wells and Coppersmith, 1994) such large displacements imply the occurrence of very large magnitude earthquakes (M 7.0–7.5). However, a c. 10 km long fault, such as this, would be expected to experience earthquakes no larger than M 5.5–6.5. One possibility is that this fault ruptures in unison with the neighbouring Magnola Fault (Schlagenhauf et al., 2011), allowing longer ruptures to form and hence larger magnitude earthquakes. Another possibility is that the cusps and soil-signature chemical bands on the fault plane are formed by periods of rapid slip containing several smaller earthquakes as pointed out by Schlagenhauf et al. (2011). It is clear that the ability to differentiate between these possibilities is desirable, but before we can be confident that the cusps interpreted from the ^{36}Cl data are robust we must confirm the relative contributions of fault slip, erosion/sedimentation and landslide activity to exhumation of the fault plane.

2.2. The Fiamignano Fault

The Fiamignano Fault system (Fig. 1) is a c. 30 km-long NW–SE trending normal fault with structural and geomorphic features similar to those observed on the Magnola Fault. The presence of a significant bedrock scarp that places deformed Mesozoic limestones against Quaternary/Holocene sediments, has led to interpretations of the existence of an active fault near the town of Fiamignano (Morewood and Roberts, 2000; Guerrieri et al., 2002; Roberts and Michetti, 2004; Papanikolaou et al., 2005; Faure Walker et al., 2010). The fault scarp exhibits a c. 20 m vertical displacement of the last glacial maximum surface across the central portion of the fault, for which an age of 15 ± 3 ka is assumed. Using this value, a throw-rate of 1.1–1.7 mm/yr is inferred (Faure Walker et al., 2010) with a lateral reduction in this rate towards the fault tips. This decrease in throw rate is consistent with a measured decrease in total throw over a similar along-strike distance along the fault (Morewood and Roberts, 2000; Roberts and Michetti, 2004), although at least some of this throw is probably inherited from extension dating from Miocene times (Bigi and Costa Pisani, 2003).

Recent earthquake activity on this fault is consistent with severe localised damage that occurred near this fault in one of the three 9th September >M 6 1349 A.D. earthquakes (Guerrieri et al., 2002). Other authors propose an alternative hypothesis whereby seismic activity on this fault ceased in the Mid-Pleistocene (Galadini, 1999; Galadini and Messina, 2001), with scarp activity, manifested by the rotation of slope-derived breccias of early Pleistocene age, being solely related to deep-seated gravitational movements (Galadini and Messina, 2001). It has also been suggested by Bigi and Costa Pisani (2005) and Bigi et al. (2003) that the Fiamignano fault controlled sedimentation during the Tortonian–early Messinian foredeep stage of Apennine thrusting. With a history of large earthquakes in the region, it is critical to highlight the importance of a full geomorphological assessment when dismissing or accepting the potential for >M 6.3 earthquakes on this fault.

2.3. Tre Monti

The Tre Monti normal fault (Fig. 1) is the WSW–ENE striking neighbour of the Magnola Fault with a bedrock fault scarp traceable for 6–7 km offsetting the 15 ± 3 ka peri-glacial surface by 3.6 m (Morewood and Roberts, 2000). The scarp has developed oblique to the NW–SE trend of the Apennine array with a geometry consisting of small overlapping segments. The implied rate of throw accumulation is 0.24 ± 0.06 mm/yr. We know of no paleoseismic studies of this fault and as such it remains unclear whether this fault is similarly activated in earthquakes like the 1915 Avezzano earthquake (M 6.9–7.0), located 10–20 km to the SE. It is therefore essential to assess the geomorphology of this site to address whether this short WSW–ENE striking fault ruptures contemporaneously with or independently of other larger normal faults that strike NW–SE.

3. Method and data

3.1. Terrestrial laser scanning

Terrestrial laser scanning or TLS is a ground-based form of light detection and ranging (LiDAR). Pulse based laser scanners, such as the Riegl LMS-z420i used in this study, operate by emitting a laser pulse at a known azimuth and angle of inclination relative to the scanner. The time of flight of an emitted pulse and its reflected, returning counterpart is used to calculate the distance between the tripod-mounted laser scanner and a surface. By emitting thousands of pulses per second and incrementally adjusting the direction, horizontally and vertically the scanner is able to sample reflections within its 360° horizontal, 90° vertical line of sight (Wilkinson et al., 2010), producing a 3D point cloud based on the Cartesian coordinates (x, y, z) of reflected points. Point cloud datasets represent an accurate representation of the real world landscape with point spacing of 10 mm at 100 m range and hence can be used for topographic analysis including the identification of tectonic and geomorphic features. Other applications of the technology are broad and extensive, but within the fields of tectonics and geomorphology include the measurement of successive micro-scale, postseismic surface motions by repeat data acquisition over a survey time span (Wilkinson et al., 2010, 2012) as well as progressive hard rock coastal cliff erosion (Rosser et al., 2005).

The point cloud datasets for this study were gathered from the Fiamignano, Tre Monti and Magnola fault scarps using multiple scan positions linked by reflector targets, located with DGPS, to gain line of sight coverage along the length of the exposed scarp (see Table 1 and Fig. 1). The acquired point cloud datasets for each scarp were then processed using the GEON points 2 grid (P2G) utility (Kim et al., 2006), which is able to act as a pseudo-vegetation filter. For each point cloud dataset to be processed within the P2G utility, a desired output is defined as a regular spaced grid in map view (i.e. 4 m), as well as a search radius and a minimum filter. For each point on the output grid the P2G utility calculates the minimum value in the z direction, which is available from the points of the input dataset, which lie within the specified search radius. The product is the removal of the unwanted laser returns, which occurred from vegetation situated above the ground surface. The resultant calculated points are output as a raster, which is then converted back into a pointset using the export to *xyz* feature in Global Mapper. The vegetation-filtered point cloud is then interpolated to represent

Please cite this article as: Bubeck, A., et al., The tectonic geomorphology of bedrock scarps on active normal faults in the Italian Apennines mapped using combined ground penetrating..., Geomorphology (2014), http://dx.doi.org/10.1016/j.geomorph.2014.03.011

Table 1
TLS survey attributes and the resultant processing output from the Points 2 Grid utility.

Fault	No. of scan positions	Along strike length of scarp acquired (m)	Total point count for point cloud dataset	Output P2G point cloud (map spacing [m]/point count)
Fiamignano	6	880	13,350,561	4/27,632
Tre-Monte	2	620	12,826,084	1/279,851
Magnola	2	230	12,472,417	4/15,404

the surface topography using the Discrete Smooth Interpolator command in GoCAD (DSI, Mallet, 1992), which operates to produce a smooth triangulated mesh from an input pointset. The created surface was carefully analysed to identify geomorphic and tectonic features by computing and displaying the dip of each mesh triangle on a colour map scale, as well as producing cross sections through the surfaces. Topographic contours were derived from the resultant surfaces using the contour tool within the spatial analyst extension of ArcGIS.

3.2. Ground penetrating radar

Previous GPR studies in the central Apennines (Salvi et al., 2003; Bristow and Jewell, 2004; Roberts et al., 2010) have been concerned with the location and analysis of paleoseismic trench sites as well as establishing fault plane continuity at depth, subsurface structures associated with earthquake surface ruptures and the shape and displacement of buried landforms.

GPR is a non-destructive method that interprets changes in the dielectric properties of the subsurface to determine structures and layering, which may not be identifiable from surface observations. It operates by sequentially emitting high-frequency electromagnetic (EM) pulses of energy from a transmitting antenna into the ground. Upon entering the subsurface the radar wave undergoes a velocity change related to variations in dielectric and electric properties of a material at a discontinuity (Conyers and Goodman, 1997; Reynolds, 1997). Here, some of the emitted energy is reflected and the other portion is lost. Upon return to the receiving antenna, the detected signals are amplified and displayed on a computer screen as a function of their two-way travel time, enabling in-field visualisation of a cross sectional radar trace. Significant reflections are produced by changes in the following; fluid content, grain type, packing and changes in the bulk density at a stratigraphic boundary (Conyers and Goodman, 1997; Neal, 2004). Propagation capabilities of the GPR wave are site specific and depend heavily on the frequency of the emitted signal and the electrical properties of the subsurface. The relationship between signal loss and antenna frequency means that, typically, a higher frequency antenna will achieve a lower maximum penetration depth than a lower frequency antenna but at a higher resolution (for more detail please refer to Neal, 2004). The most successful GPR datasets are derived from shallow, electrically resistive materials that are dry and free from high conductivity deposits such as clay, which will rapidly reduce penetration depths from ~30 m to a few metres (Olhoeft, 1998).

For this study, we operated a Sensors and Software PE-100 GPR system in common offset profiling mode. For the acquisition of high-resolution data we used 200 MHz antenna with a separation distance of 0.5 m and a step size of 0.1 m. According to wave theory, the highest achievable vertical resolution of the survey is one quarter of the operating wavelength (Jol and Bristow, 2003). Using the setup described above we can calculate an ideal vertical resolution of 0.125 m (assuming an average pulse velocity of 0.1 m/ns and dry conditions). However, this value represents the best that can be achieved; in reality the resolution will be slightly less owing to the complexity of ground responses.

Raw radargrams were processed using a common workflow but with varying parameter values due to favourable conditions at all sites. Data processing included time-zero correction, de-wow filtering, bandpass filtering and automatic gain control application to boost signals at depth. To determine average wave velocities a common mid-point (CMP) survey was conducted perpendicular to the survey lines and parallel to the fault planes. The results from these surveys give an approximate average pulse velocity of 0.1 m/ns, comparable to values obtained from the profile data using the shape of diffraction hyperbolae. This value was used to apply the topographic correction to the processed radargrams. Further details on the applications and processing procedures of GPR are presented by Neal (2004), Schrott and Sass (2008) and Jol and Bristow (2003). We were able to collect GPR data for the Fiamignano and Tre Monti fault scarps, but not the Magnola Fault scarp, where the subsurface was visible to an extent due to the presence of large hangingwall gully c. 100 m to the SE of the ^{36}Cl cosmogenic dating site of Palumbo et al. (2004) and Schlagenhauf et al. (2010, 2011).

3.3. Integration of TLS topography with GPR reflection profiles

Two GPR surveys were conducted perpendicular to the Fiamignano Fault. Both surveys start at the base of the scarp and extend southwest across the hangingwall. Fiamignano (1) extends 30.8 m and Fiamignano (2) 84.3 m. At Tre Monti, four GPR surveys were conducted perpendicular to the fault scarp. All of the surveys begin at the base of the scarp and extend 25–30 m across the hangingwall in a southerly direction. As the GPR is incapable of detecting changes in topography, the initial reflection profile is assumed to have been conducted across a level horizontal surface (Fig. 2a), which without applying surface topography, bears little relation to the subsurface geometry. Traditionally, topographic data are gathered along GPR survey lines using either GPS or total station measurements, with map spacing between successive measurements dependent on line length, but commonly between 1 and 10 m. However, by creating cross sections through the acquired TLS datasets corresponding to the GPR survey traces, we are able to extract detailed topographic profiles (Fig. 2b). Map spacing of surface measurements from this method are typically between 0.1 and 0.5 m. The application of TLS derived topographic profiles to the GPR reflection profiles has allowed the production of detailed reflection profiles (Fig. 2c), where surface features can be clearly traced into the subsurface. Applying detailed TLS topography to a GPR reflection profile improves clarity and enhances subsurface features, which are commonly difficult to distinguish using traditional topographic data.

4. Results

4.1. The Magnola Fault scarp

With a variety of published ^{36}Cl and chemical data that demonstrate episodic Holocene exhumation of the fault plane (Palumbo et al., 2004; Carcaillet et al., 2008; Schlagenhauf et al., 2010), we begin with the Magnola Fault scarp, despite lacking GPR data for this location. We aim to assess whether episodic exhumation of this fault plane was a result of earthquake slip events or a combination of this and erosion, sedimentation or landsliding.

Close to the village of Forme (Fig. 1), the Magnola scarp is clear and continuous in the topography for 3.4 km along strike, forming

Please cite this article as: Bubeck, A., et al., The tectonic geomorphology of bedrock scarps on active normal faults in the Italian Apennines mapped using combined ground penetrating..., Geomorphology (2014), http://dx.doi.org/10.1016/j.geomorph.2014.03.011

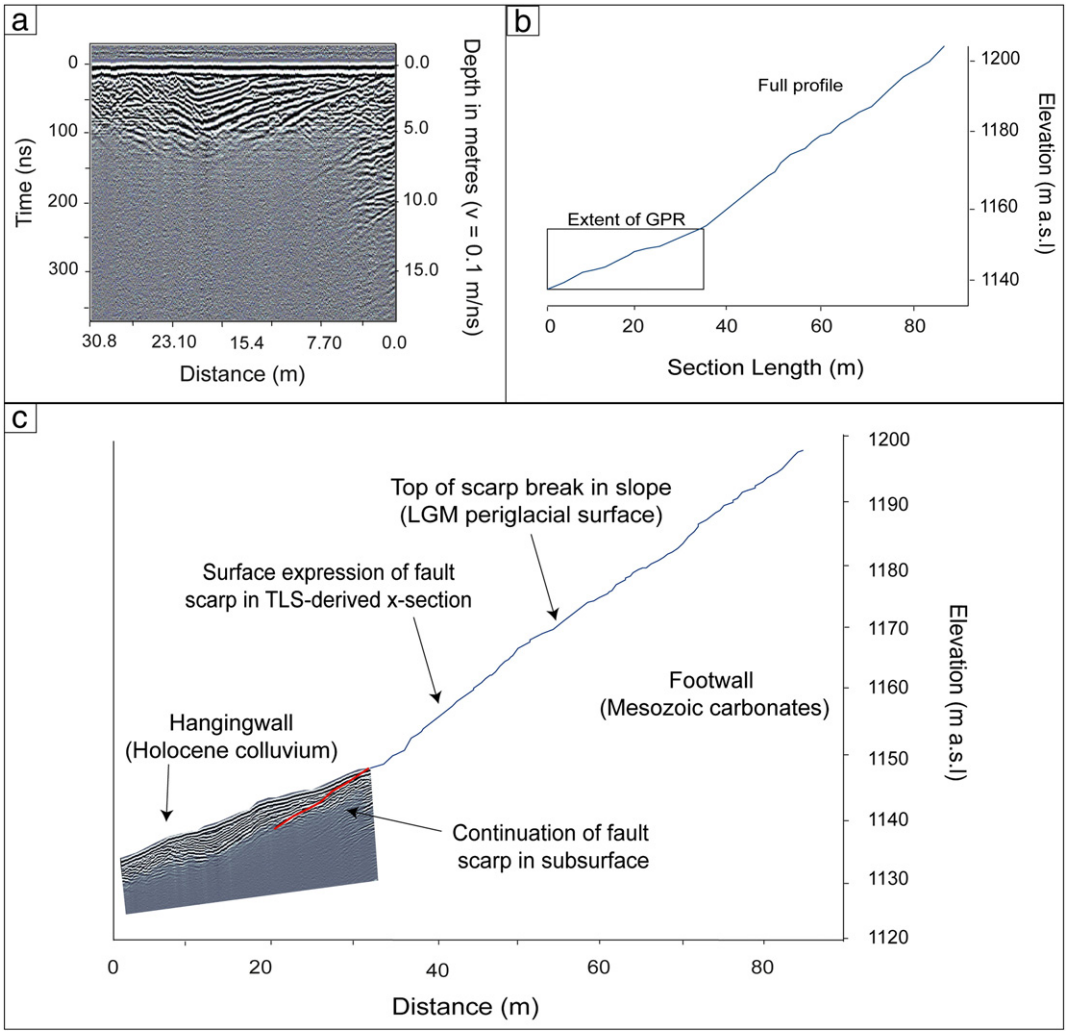

Fig. 2. (a–c): TLS-GPR integration workflow. a) GPR reflection profile without topography applied. b) TLS derived topography corresponding to the path of the GPR survey in (a) with point spacing 0.1–0.5 m. c) The final GPR profile with the TLS derived topography applied. Surface features displayed in cross section from the TLS data, such as fault scarps observed with consistent subsurface geometry within the reflection profile.

a single segment of the 10 km long Magnola Fault. A TLS-derived topographic surface was created (Fig. 3) with slope angles indicating a clear break of slope at the base of the Mesozoic limestone footwall of the fault. Here, the fault plane dips at 45° whilst above this the upper slope (footwall) is at 36°. Tucker et al. (2011) have interpreted such a change in slope angle to indicate that higher erosion rates affected the emerging scarp during the last glacial episode than in the Holocene. Earlier exhumed portions of the fault plane experienced a greater depth of erosion in the last glacial episode preventing the preservation of the fault plane during this time and resulting in lower slope angles. However, in the Holocene, lower erosion rates affected the emerging fault plane and the original slope angle is preserved as a free face.

The lower slope (hangingwall), within the polygon in Fig. 3, is located lower on the overall slope than the exposed fault plane and dips at 25°. Although this is shallower than the upper slope, the lower slope is planar and not cut by erosional gullies. The planarity of this slope suggests that it is the preserved continuation of the upper slope, produced by sedimentation associated with the high rates of erosion of the last glacial maximum (Tucker et al., 2011). Thus, it is reasonable to assume that this paleosurface has been unaffected by landsliding, erosional incision of hangingwall drainage, or burial by sediment derived from the footwall during the Holocene (Fig. 3, see polygon). This interpretation is consistent with the exposed stratigraphy within the major gully running NNE–SSW across the DEM where the layering of the hangingwall colluvial stratigraphy is parallel to the slope of the interpreted paleoground surface. Such a sedimentary geometry is consistent with those postulated to exist beneath last glacial maximum colluvial surfaces by Benedetti et al. (2002) along the Sparta fault scarp in southern Greece. This implies that the free-face Magnola Fault scarp has been exhumed solely by fault slip at the site sampled for ^{36}Cl by Palumbo et al. (2004) and Schlagenhauf et al. (2010), consistent with their conclusions.

The fault offset that has developed since the formation and preservation of the paleosurface can be measured by examining the vertical offset across the fault scarp. The base of the fault scarp (Fig. 3, dotted line) and the clear break in slope that exists at the top of the fault plane (Fig. 3, dashed line) are well defined in the white polygon, with a vertical distance between them of c. 15 ± 1 m for c. 100 m along strike within the white polygon. If the paleosurface was formed due to erosion or sedimentation associated with vigorous freeze–thaw action during the last glacial maximum (15 ± 3 ka) as we suspect, the vertical offset that has developed since then has accumulated at an average rate of 1 ± 0.07 mm/yr.

Elsewhere along the Magnola scarp near Forme, the geomorphology does not allow derivation of throw-rates in the manner described above. In the incised gully, alluvial processes have exhumed the fault

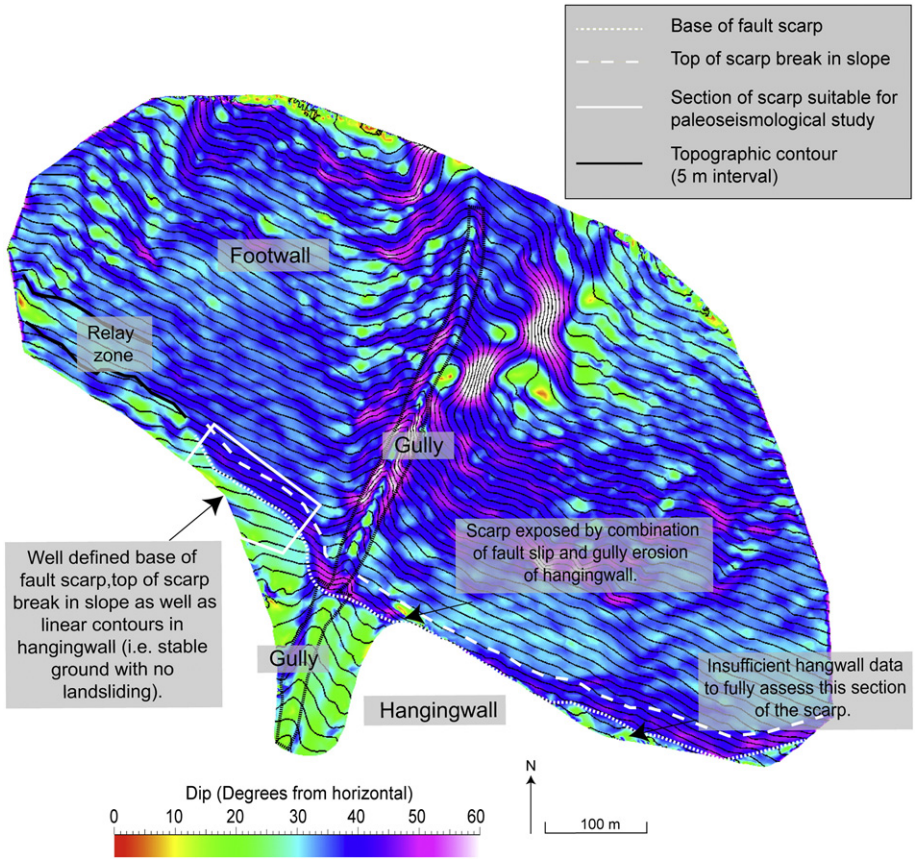

Fig. 3. Magnola surface raster coloured by slope angle, created by discrete smooth interpolation (DSI) of the points2grid *xy* minimum *z* pseudo-vegetation filter with 4 m map spacing between points output using the original TLS Magnola dataset. Darker shades represent steeper dips (for full colour, see online version of manuscript). The 5 m topographic contours shown were calculated using the *z* values from the points2grid output.

surface and further to the ESE the scarp is degraded with a poorly preserved and therefore poorly defined free face. Although the lower slope is covered by large trees, further inspection in the field shows it is marked by incised gullies, contributing to the difficulty in interpreting the vertical distance between the dotted and dashed lines. Consequently, it is unclear how to measure a reliable throw-rate to the ESE of the incised gully, as the scarp appears to have been exhumed by a combination of fault slip and hangingwall incision by slope/fluvial processes. Overall, it is possible to obtain a robust throw-rate from within the polygon we have indicated on the Magnola scarp, where the fault scarp has been exhumed by fault slip and not by erosion/sedimentation or landsliding. This conclusion supports the work of Palumbo et al. (2004) and Schlagenhauf et al. (2010, 2011) who derived in situ ^{36}Cl cosmogenic exposure ages for the fault plane within the white polygon; we believe that these exposure ages should provide a reliable record of fault plane exposure. Using the lessons learned from the Magnola scarp, we move next to the Fiamignano and Tre Monti fault scarps, respectively, where we have GPR data to complement our TLS data. Our aim is to identify surface and subsurface evidence for mechanisms responsible for fault exhumation at these two localities, to investigate whether uplift of the scarps was due to slip during earthquake events or pulsed erosion, sedimentation or landsliding.

4.2. The Fiamignano Fault scarp

A topographic surface, coloured by dip, was obtained from a TLS dataset to exhibit slope angles for a c. 800 m section of the Fiamignano Fault (Fig. 4). For this section of the fault, the surface demonstrates distinct breaks in slope, corresponding to (a) the base of the Mesozoic limestone footwall and the lower slope beneath this (Fig. 4, white dotted line), and (b) the upper slope above the fault scarp (above the dashed line in Fig. 4). The TLS-derived slope angles indicate that the fault scarp dips at 40–45° and above this the upper slope is at an angle of 30–35°. This further corroborates the suggestion by Tucker et al. (2011) that early-exhumed portions of scarps in the central Apennines underwent higher erosion rates prior to the Holocene, so that early-exhumed portions of the fault plane underwent a greater depth of erosion during the last glacial period.

Within polygon a in Fig. 4, the upper slope on the footwall is planar and free from incised gullies. It slopes at 30–35° with no evidence of significant Holocene footwall incision. Thus, we can be confident that the paleosurface from the last glacial episode remains intact. The hangingwall slope beneath the fault scarp also appears continuous and planar, sloping at 20–25°. Its planar nature and our geomorphic mapping suggest that it has been unaffected by landsliding, erosional incision, or burial by Holocene sediment derived from the footwall and represents the preserved continuation of the slope formed in the last glacial maximum. Observations of the layering within the sediments forming the lower slope would corroborate this hypothesis; a preserved paleosurface from the last glacial episode should be underlain by layers parallel to the ground surface, as seen in the incised hangingwall gully at the Magnola scarp and as postulated for such locations by Benedetti et al. (2002). A GPR profile across the lower slope in Fig. 5a and b displays regularly layered, continuous reflectors that lie parallel to the ground surface between 4 and 15 m along the profile. The regularity of these signals demonstrates a lack of disturbance by landsliding, erosional incision or burial, supporting the proposal of a tectonically exhumed fault scarp. At depth beneath these signals is a distinct, dipping reflector, which we interpret to be

Please cite this article as: Bubeck, A., et al., The tectonic geomorphology of bedrock scarps on active normal faults in the Italian Apennines mapped using combined ground penetrating..., Geomorphology (2014), http://dx.doi.org/10.1016/j.geomorph.2014.03.011

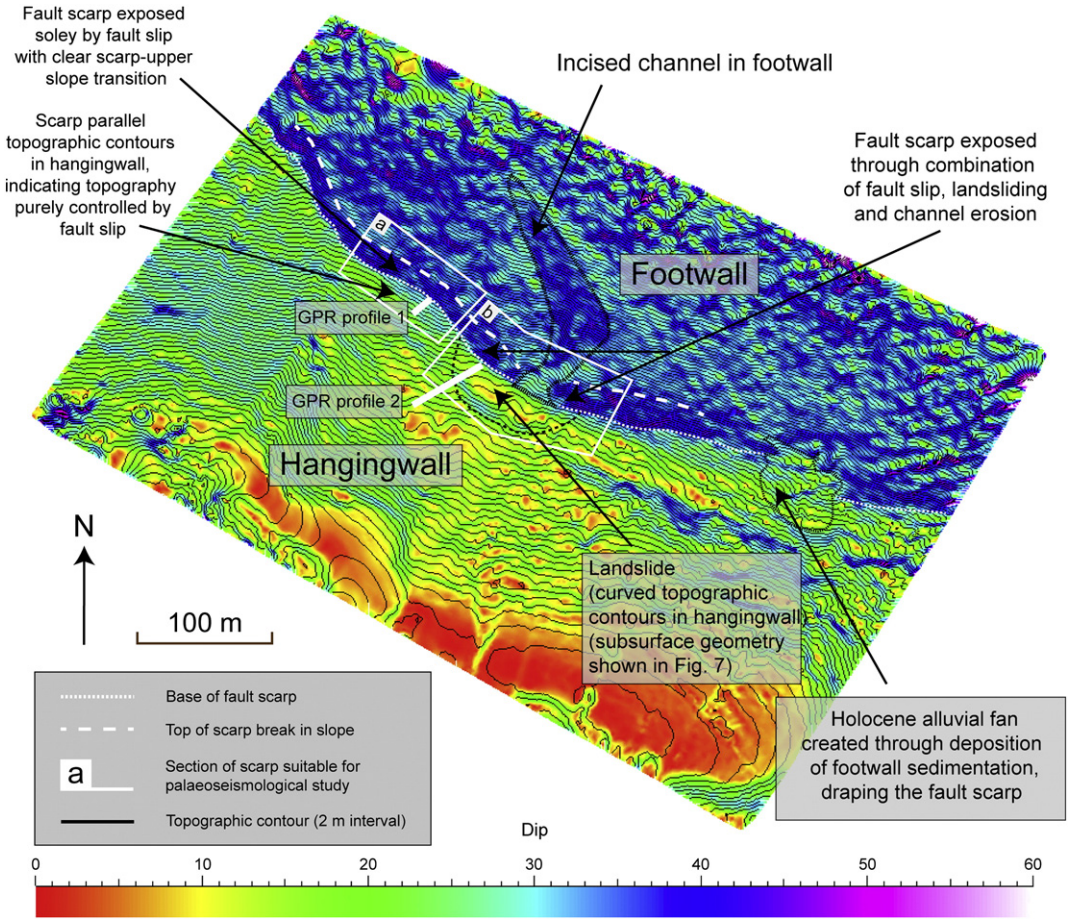

Fig. 4. Fiamignano surface raster coloured by slope angle, created by discrete smooth interpolation (DSI) of the points2grid *xy* minimum *z* pseudo-vegetation filter with 4 m map spacing between points output using the original TLS Fiamignano dataset. Dark shades are steeply dipping and lighter shades are shallow dipping.

the subsurface continuation of the fault plane (dashed line, Fig. 5b) and represents the interface between the electrically resistive limestone of the footwall and the less resistive hangingwall sediments.

Between 15 and 25 m from the fault scarp we note the presence of reflector geometries suggestive of a fold, but we interpret this to be anthropogenic disturbance. 10 m along strike from this feature to the SE we note the presence of a degraded stonewall that probably formed a field boundary. The orientation of the wall suggests it may have originally continued to the NW to cross the site where our GPR data show a fold-like structure. We also note that this fold-like feature has no apparent surface expression, examined in the field by eye or within the TLS data at this location. Thus, we believe the structure is due to anthropogenic disturbance of the site during construction of the wall.

We conclude therefore, that the fault offset across this section of the Fiamignano Fault has developed since formation and preservation of the paleosurface, satisfying the criteria for reliable throw-rate calculations, which may be achieved by measuring the vertical offset across the fault scarp. Using the well defined fault scarp base and upper slope a vertical distance of c. 19 ± 1 m for a c. 100 m section of the fault within polygon a and an assumed age of the paleosurface of 15 ± 3 ka, the offset has accumulated at an average rate of 1.27 ± 0.4 mm/yr.

In contrast, within polygon b, the nature of the geomorphology differs considerably from the previous site and prevents derivation of robust throw-rates. The presence of an incised gully in the footwall (Fig. 4, heavy black line) is noted midway along the investigated section of the scarp and cuts back significantly into the footwall by tens of metres implying the footwall paleosurface is no longer intact. It is evident that this incision does not continue into the hangingwall, suggesting that Holocene sedimentation has affected the hangingwall. A low hangingwall surface slope (~10°) exists in this location captured by the LiDAR slope map (Fig. 4), consistent with our suggestion that the last-glacial maximum paleosurface has been covered by hangingwall sediment. This accumulation of sediment is associated with a flat-topped area that is surrounded downslope by a steep scarp on the lower slope. This scarp has a lenticular shape in map view, reminiscent of a toe-scarp to a rotational landslide. This possible rotational landslide was tentatively identified in the field by eye, and its extent is highlighted in polygon b (Fig. 4) by a black dotted line. We conducted a GPR survey to test the landslide hypothesis. The GPR data from this site are significantly different to the previous site with reflectors displaying geometries that are discontinuous and disrupted, dipping NE back towards the fault plane rather than parallel to the ground surface as in polygon a (see Fig. 6 a and b). This suggests that hangingwall Holocene sediment has undergone rotational slip transporting material down and outwards, away from the fault plane. Thus, the sub-horizontal bench in the hangingwall with lenticular map geometry indicated by the black dotted line in Fig. 4 is the surface expression of a rotational landslide with dimensions of ~100 m along strike and ~30 m across strike. This landslide is likely to have contributed to surface exposure of the carbonate fault plane. The continuation of the carbonate fault plane in the subsurface is likely to be represented by a strong reflector dipping SW, which is produced by the lithological change from Pleistocene sediments in the hangingwall to the carbonate footwall. Numerous spatially limited hyperbolic features with dimensions smaller than one wavelength of the radar wave are also present between 54 and 69 m, producing minor interference in the traces; these may indicate the

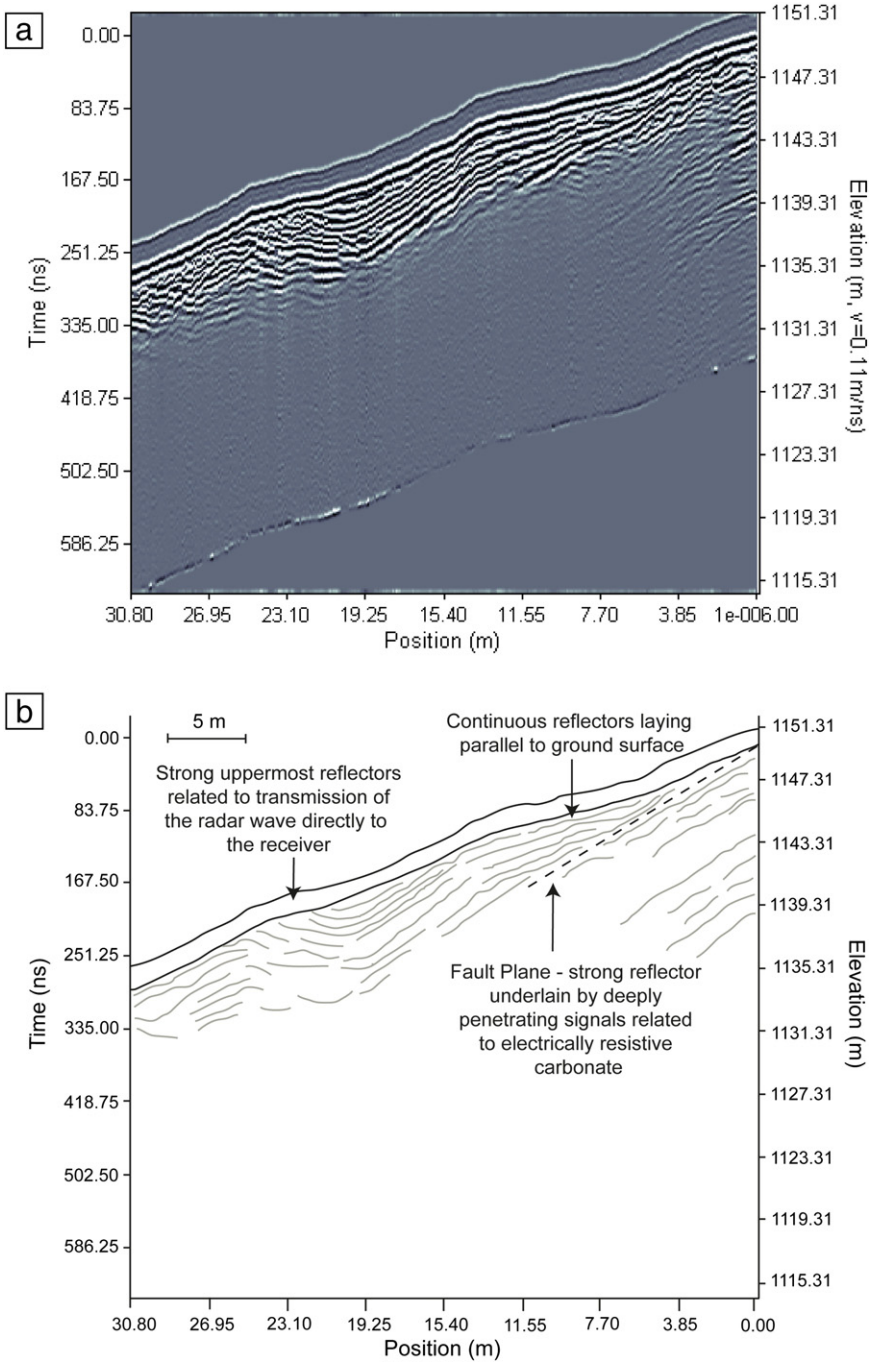

Fig. 5. a) A GPR profile along transect 1 (see Fig. 6) on the hanging wall of the Fiamignano Fault with TLS topography applied. b.) Interpretation of GPR profile. Facies show clear layered reflectors that lie parallel to the ground surface. We attribute the uppermost reflectors to the transmission of the radar wave directly to the receiver across the ground surface and in the immediate subsurface (solid black lines).

presence of large clasts or boulders in the sub-surface (Jol and Bristow, 2003).

With evidence for incision, sedimentation and landslide activity in polygon b, we conclude that throw rates and earthquake slip histories should not be derived at this site without careful consideration of the geomorphology. This contrasts with the conclusions of Benedetti et al. (2013) who use ^{36}Cl data to derive the ages of individual earthquakes without discussion of how to factor in the complex geomorphology. However, within polygon a, the fault scarp has been exhumed solely by fault slip and is suitable for the calculation of robust throw-rate measurements across the scarp and study with ^{36}Cl exposure dating. The comparison of these sites highlights the variety of geomorphic features that exist along this fault over a distance of a few hundred metres.

4.3. The Tre Monti Fault scarp

Our TLS-derived topographic surface for the Tre Monti Fault demonstrates slope angles for a c. ~700 m portion of the fault that we separate into 3 sections based on the geomorphology and sedimentation (Fig. 7, polygons a, b and c). As with the previous localities, we observe areas of the fault where reliable measurements of throw-rate can be obtained and others where such measurements are not possible. In all 3 polygons, the fault exhibits a clear break in slope at the base of its Mesozoic

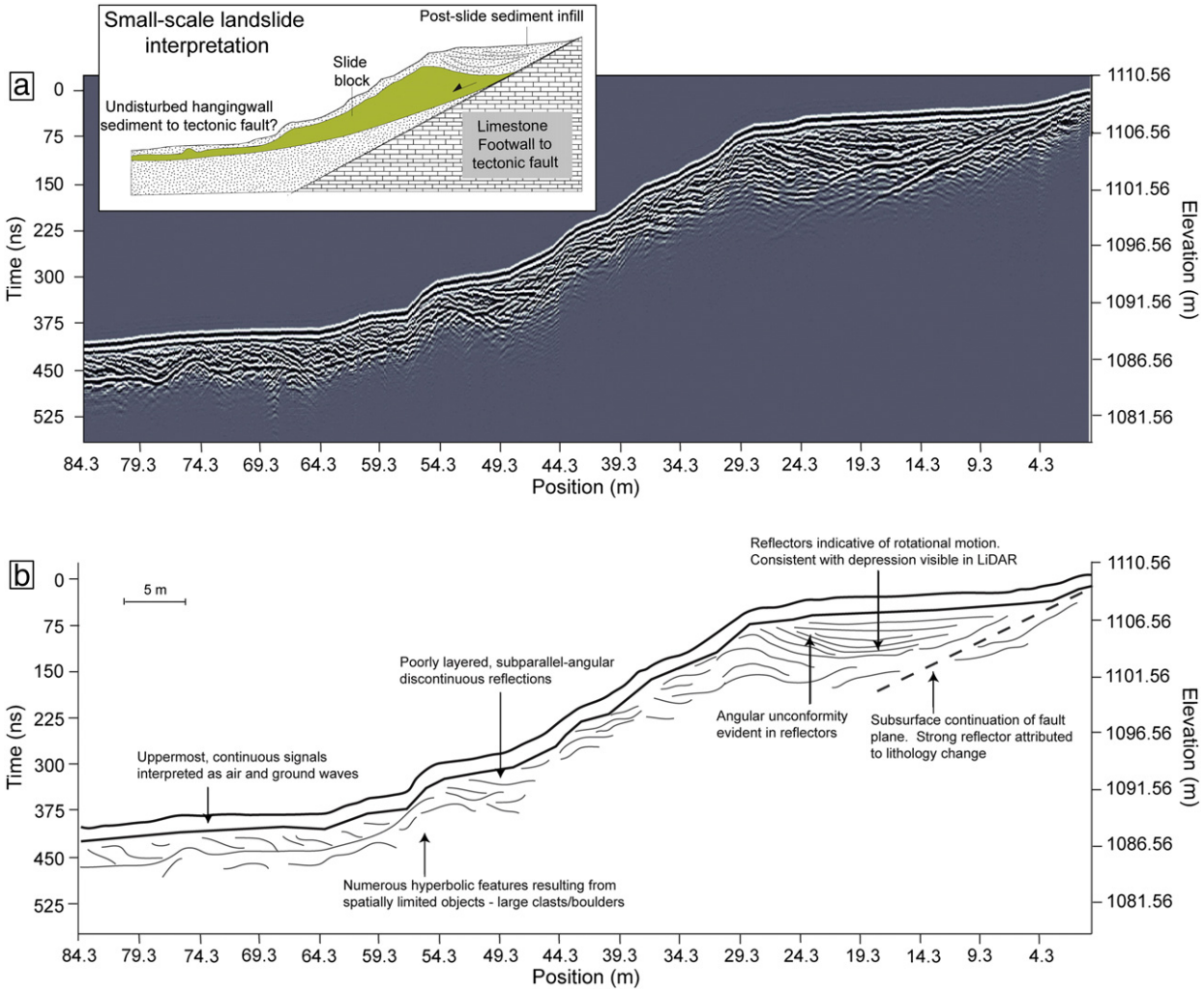

Fig. 6. a.) A GPR profile along transect 2 (see Fig. 4) on the hanging wall of the Fiamignano Fault with LiDAR topography applied. b.) Interpretation of GPR profile. Between 5 and 35 m, to a depth of ~10 m, the reflectors exhibit geomorphic geometries consistent with gravitational movements.

limestone footwall and another break at the top of the fault scarp where it meets the upper slope. The TLS surface provides slope angles for the fault scarp in polygons a, b and c of 40–45°, and the upper slope in these regions of 35–40°.

Polygon a is characterised by a lower slope exhibiting consistent slope angles of ~25°. The fault scarp displays a pronounced left-step which we interpret as a relay zone. This relay zone has acted as a pathway for the transport of sediment from the footwall to the hanging wall, evidenced by a small alluvial fan in the apex of this relay zone. The fan displays greater slope angles than the lower slope (up to 30–35°), and is also evident in GPR transect 1 (Fig. 8). The fan, which is clearly visible at the surface as a subtle convex upwards cone of colluvium emanating from a feeder channel on the footwall, appears between 16 and 22 m as a small wedge-shaped package of reflectors at depth deposited at the base of the scarp; internal reflectors dip towards the fault plane. Elsewhere in polygon a, the fan has not affected the lower slope. The planarity and preservation of the lower slope away from the fan implies it is the downthrown continuation of the upper slope and thus is also produced during sedimentation associated with the high rates of fault zone erosion during the last glacial episode. The contours in the hangingwall of polygon b are parallel to the strike of the fault and suggest slope angles of 25–30°. This lower slope is similarly planar, suggesting that it is also unaffected by incision, erosion, sedimentation and landsliding during the Holocene. This is consistent with three additional GPR profiles that lie perpendicular to the strike of the fault in this polygon (Fig. 8, transects 2–4). Throughout these profiles we observe continuous, linear hangingwall reflectors lying parallel or sub-parallel to the ground surface. Radar facies exhibit strong reflective patterns in sediments that presumably date from the last glacial maximum, underlain by a strong reflector that we interpret to be the limestone fault plane. The hangingwall is also seen to be free from faulting in both the TLS and GPR datasets, suggesting there is no evidence for a breaching fault across the relay zone and as such, all of the strain in this area has been accommodated on the carbonate fault plane. The upper slope is also planar and unaffected by the incision of footwall gullies, consistent with our interpretation that it is composed of sediments from the last glacial maximum, and not Holocene sediment.

In polygon c, lower slope angle values vary significantly and curved contours clearly indicate the existence of a large depression (Fig. 7, heavy black dashed line),that is incised by erosional gullies. The nature of the lower slope in this section of the fault is such that that it cannot be reliably interpreted as the continuation of the upper slope. Instead, we interpret the depression to be the surface manifestation of a large landslide that is several hundred metres across.

We propose that the amount of vertical offset across the fault in polygons a and b, like the first sites at Magnola (polygon, Fig. 3) and Fiamignano (polygon a, Fig. 4), has developed since the formation and preservation of the last glacial maximum paleosurface, except where the fan is located in the relay zone. Clearly defined,

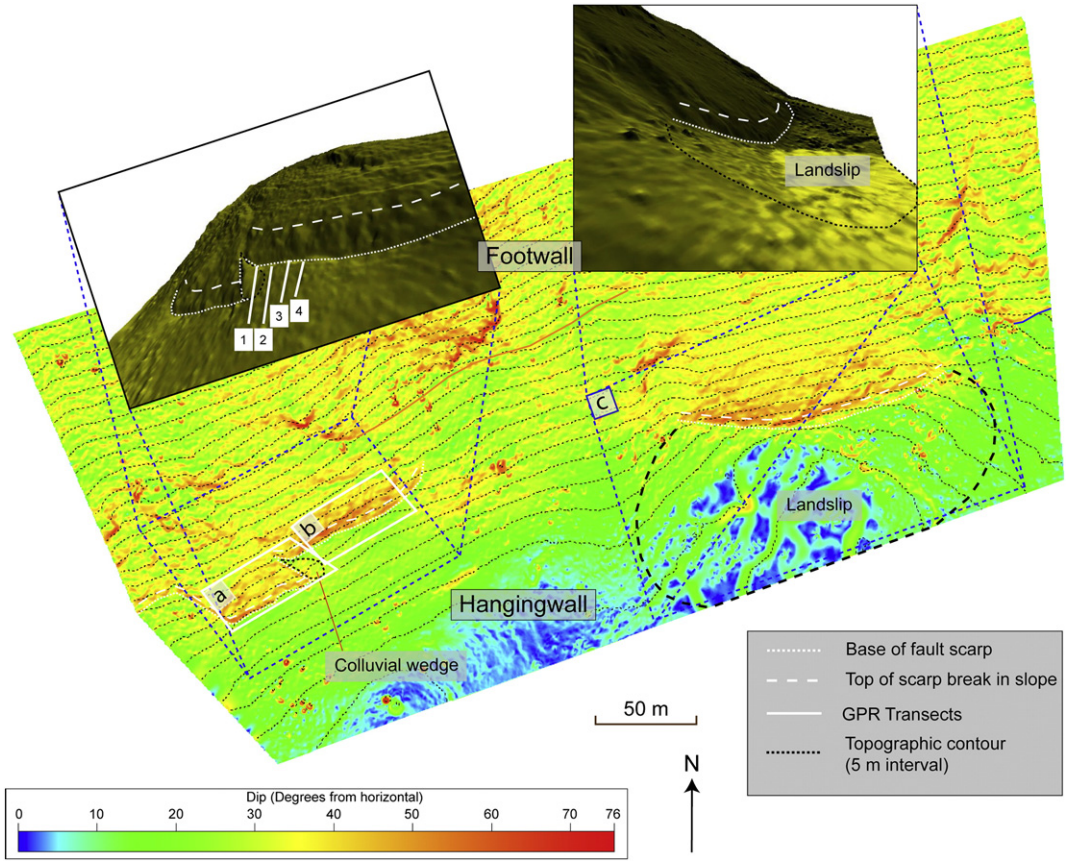

Fig. 7. Tre Monti surface raster coloured by dip, created by discrete smooth interpolation (DSI) of the points2grid *xy* minimum *z* pseudo-vegetation filter with 1 m map spacing between points output using the original TLS Tre Monti dataset. The 5 m topographic contours shown were calculated using the *z* values from the points2grid output.

well-preserved breaks in slope exist at the top and bottom of the fault scarp (Fig. 7, dashed and dotted lines respectively) permitting well-constrained calculations of fault throw rate. The vertical distance between the upper and lower slope is c. 6.5 ± 1 m for each 80 m section of the fault in polygons a and b. If the paleosurface was produced by erosion or sedimentation related to freeze thaw action during the last glacial episode (15 ± 3 ka), the vertical offset across the fault has developed at an average rate of c. 0.43 ± 0.067 mm/yr. Elsewhere in polygon c the geomorphology does not permit the calculation of robust throw rates. In this area exposure of the fault scarp is attributed to a combination of fault slip and slope destabilisation resulting in landslides.

In summary, it is possible to obtain reliably constrained throw rates from within polygons a and b on the Tre Monti scarp where it has been exhumed by fault slip and not influenced by erosion, landsliding or sedimentation; these sites are suitable for study with ^{36}Cl exposure dating.

5. Discussion

Varying interpretations of scarp-forming processes exist in the central Apennines, resulting from the challenges in distinguishing the different mechanisms contributing to both subsurface and surface slope geometry (Fig. 9). Here we present a comprehensive method for characterising the various fault-scarp forming mechanisms and emphasise that surficial geological and geomorphological observations alone produce a less than complete characterisation of the evolution of fault scarps.

We present evidence supporting tectonic exhumation of specific portions of the Magnola, Tre Monti and Fiamignano fault scarps manifested by a clear base of scarp contact and upper slope to fault-scarp contact, which are undisturbed by erosion or sedimentation. These sections are commonly very limited in along-strike extent (a few tens of metres) along the scarps, and require careful observation to identify them. The transition from these zones to areas that have been exposed by non-tectonic processes, as a result of geomorphic exhumation processes can occur over distances of a few tens of metres or less. In these areas, dominated by non-tectonic processes, we note the presence of landsliding, channel incision and sedimentation, and conclude that evidence of Holocene slip is not preserved intact and robust paleoseismological interpretations will be very challenging or impossible to obtain.

Assessment of seismic hazard is fundamentally controlled by the rate at which faults slip, because average recurrence intervals decrease as slip rates increase (Roberts et al., 2004). The reliability of slip-rate based assessments is complicated when recurrence intervals on faults are longer than the historical record of seismicity and when we consider the likelihood of temporal clustering of earthquakes on faults. To fully characterise the seismic hazard of faults an extensive record of slip is necessary (Cowie et al., 2012). The development of ^{36}Cl in situ cosmogenic dating of emergent fault planes has provided a means of obtaining records of the magnitude and timing of paleoearthquakes, as well as their recurrence intervals, spanning multiple seismic cycles. This method is best suited to bedrock fault scarps such as those described in this paper. However, this paper demonstrates that site characterisation is essential to exclude sites where geomorphic processes such as footwall fluvial/debris-flow incision, hangingwall sedimentation and landslide activity have contributed to exhumation of fault planes. Our study shows that some, but not all sites that have been studied with ^{36}Cl in situ exposure dating are suitable for deriving Holocene slip and earthquake histories.

Please cite this article as: Bubeck, A., et al., The tectonic geomorphology of bedrock scarps on active normal faults in the Italian Apennines mapped using combined ground penetrating..., Geomorphology (2014), http://dx.doi.org/10.1016/j.geomorph.2014.03.011

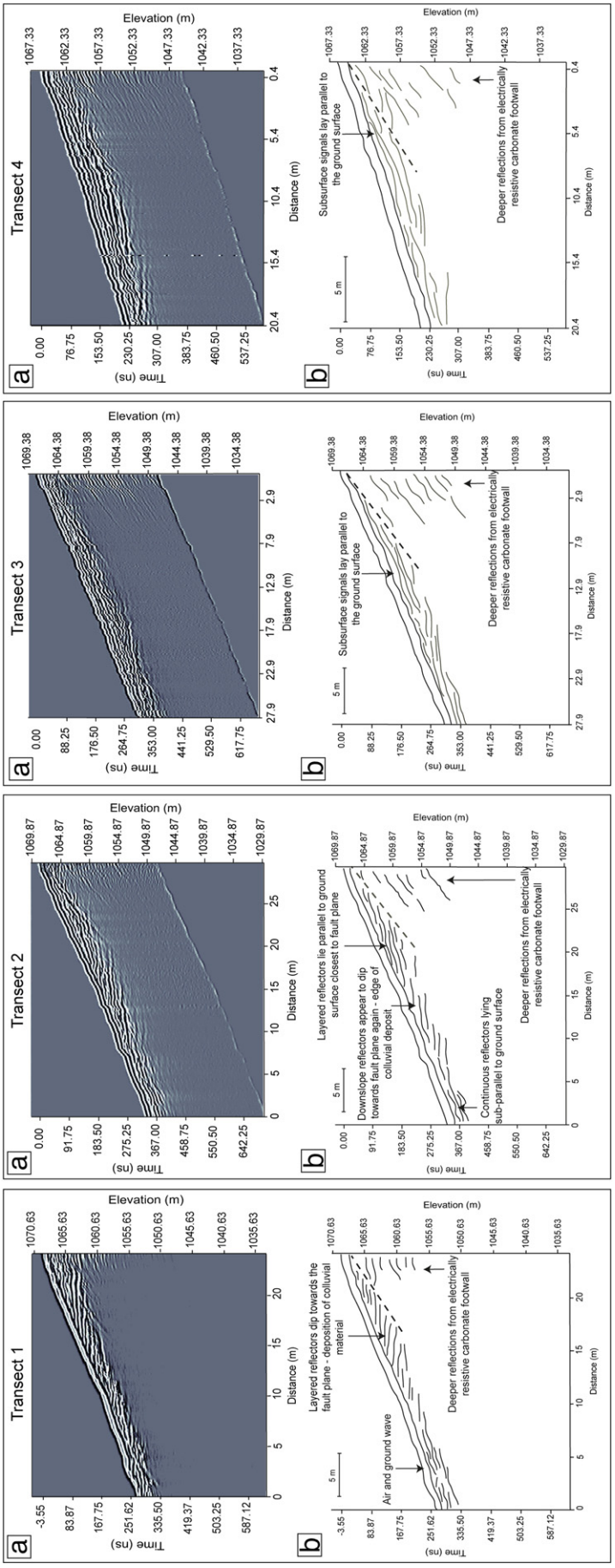

Fig. 8. GPR transects 1–4 collected across the hangingwall of the Tre Monti Fault (see Fig. 7) and interpretations with a LiDAR-derived topographic correction applied. The subsurface continuation of the fault scarp (dotted line) is traced into the subsurface at each site. Deeper penetrating signals, dipping parallel to the inferred fault planes, are returning from the electrically resistive carbonate footwall. Profile 1 demonstrates a package of reflectors that dip back towards the fault plane, representing a wedge of footwall-derived material. Profile 2 displays regular, surface-parallel reflectors between 0–7 m and 17–30 m. Between 7 and 17 m, reflectors appear to be oblique to the surface and dip towards the fault plane suggesting they may be associated with colluvial deposition. In profiles 3 and 4 continuous, undisturbed, surface-parallel reflectors suggest tectonic exhumation alone is responsible for scarp exposure in this polygon. There is no evidence that colluvial deposition affects this section of the scarp. Radar signals associated with the transmission of the transmitted signal directly to the receiver on the ground surface and in the immediate subsurface are highlighted by the two continuous bands on the surface of each profile.

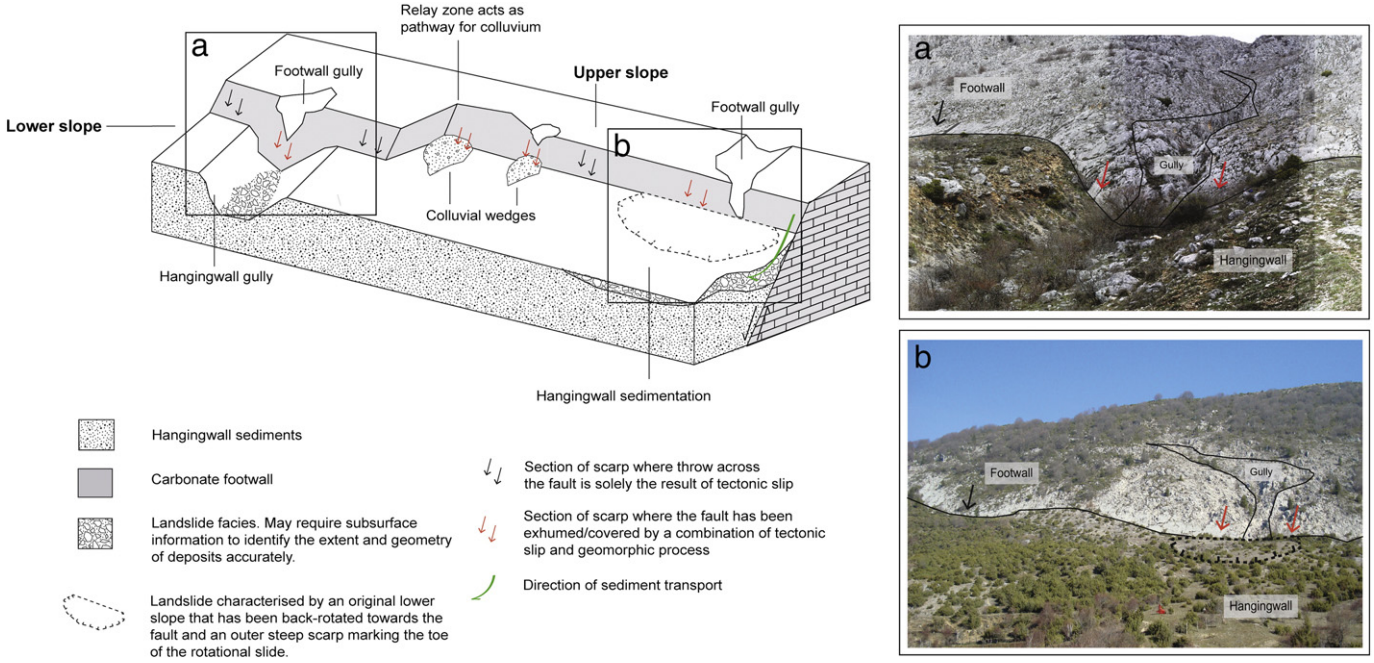

Fig. 9. Summary of processes contributing to scarp exposure in the central Apennines.

This study has highlighted the variety of tectono-geomorphic features that exist and their variation across relatively small distances. As such, we emphasise the need of careful planning when considering sites for paleoseismological studies; the implications of poor siting of study sites are severe for hazard assessment in the region. We advocate thorough investigation using remote sensing techniques such as LiDAR combined with GPR at paleoseismological study sites to fully constrain the type, extent and distribution of scarp forming processes.

6. Conclusion

The reliability of Holocene fault slip rates derived from the interpretation of bedrock fault scarps that have formed since the last glacial maximum relies heavily upon robust site selection due to the variety of tectonic and geomorphic processes that combine to exhume the fault plane. Sites that are suitable for interpretation of slip-rates display the following attributes:

1) The upper and lower slopes in the footwall and hangingwall of the fault plane must be planar and free of erosion associated with fluvial and debris flow processes that can produce incised gullies. Thus, the last glacial maximum paleosurface, that is, the upper and lower slopes must be intact.
2) The lower slope in the hangingwall must be free of post last glacial maximum sediments. Thus, the elevation values of the lower slope must not have been modified by sedimentation associated with alluvial fans or colluvial wedges.
3) The upper parts of fault plane may or may not be fully preserved. If the upper part of the fault plane is eroded, the dip of the fault plane can be extrapolated upwards to intersect the downward extrapolation of the upper slope. The implied line of intersection between the upper slope and fault plane should be parallel to the line of intersection between the fault planes and the lower slope.
4) If relay zones are present, slip-rates can only be determined from the offset of last glacial maximum surfaces if it can be demonstrated that earthquakes ruptures have not crossed the relay-zone in the hangingwall of the bedrock fault scarps.

We suggest that a combination of GPR and TLS data are the best way to constrain the four attributes listed above and we have provided examples from three Apennine fault scarps. Characterisation of the distribution and influence of the various scarp forming processes allows the production of a suitable framework for accurate slip-rate based assessments of the long term hazards posed by normal faults in the Apennines. It is also a desirable pre-requisite for site selection if ^{36}Cl in situ cosmogenic dating is to be used to constrain the recurrence of paleoearthquakes.

Acknowledgements

This study was funded by NERC grants NE/I024127/1, NE/H003266/1 and NE/E01545X/1. We thank the following for discussions of this topic: Ioannis Papanikolaou, Joanna Faure Walker, Alessandro Michetti and Eutizio Vittori.

References

Allen, J., Brandte, U., Brauer, A., Hubbertens, H.-W., Huntley, B., Keller, J., Kraml, M., Mackensen, A., Mingram, J., Negendank, J., Nowaczyk, N., Oberhansli, H., Watts, W., Wulf, S., Zolitschka, B., 1999. Rapid environmental changes in southern Europe during the last glacial period. Nature 400, 740–743.

Anderson, H., Jackson, J., 1987. Active tectonics of the Adriatic region. Geophys. J. Roy. Astron. Soc. 91, 937–983.

Attal, M., Tucker, G.E., Whittaker, A.C., Cowie, P.A., Roberts, G.P., 2008. Modeling fluvial incision and transient landscape evolution: influence of dynamic channel adjustment. J. Geophys. Res. 113, F03013. http://dx.doi.org/10.1029/2007JF000893.

Attal, M., Cowie, P.A., Whittaker, A.C., Hobley, D.E.J., Tucker, G.E., Roberts, G.P., 2011. Testing fluvial erosion models using the transient response of bedrock rivers to tectonic forcing in the Apennines, Italy. J. Geophys. Res. Earth Surf. 116, F02005. http://dx.doi.org/10.1029/2010JF001875.

Benedetti, L., Finkel, R., Papanastassiou, D., King, G., Armijo, R., Ryerson, F., Farber, D., Flerit, F., 2002. Post-glacial slip history of the Sparta fault (Greece) determined by ^{36}Cl cosmogenic dating: evidence for non-periodic earthquakes. Geophys. Res. Lett. 29, 8. http://dx.doi.org/10.1029/2001GL014510.

Benedetti, L., Manighetti, I., Gaudemer, Y., Finkel, R., Malavieille, Pou, K., Arnold, M., Aumeitre, G., Bourles, D., Keddadouche, K., 2013. Earthquake synchrony and clustering on Fucino faults (central Italy) as revealed from in situ ^{36}Cl exposure dating. J. Geophys. Res. Solid Earth. http://dx.doi.org/10.1002/jgrb.50299.

Bigi, S., Costa Pisani, P., 2003. The pre-thrusting Fiamignano normal fault. Boll. Soc. Geol. It. 122, 267–276.

Bigi, S., Costa Pisani, P., 2005. From a deformed Peri-Tethyan carbonate platform to and fold-and-thrust-belt: and example form the central Apennines (Italy). J. Struct. Geol. 27, 523–539.

Bigi, S., Pisani, P.C., Tavarnelli, E., Calamita, F., Paltrinieri, W., 2003. The pre-thrusting Fiamignano normal fault. Boll. Soc. Geol. Ital. 122, 267–276.

Boncio, P., Pizzi, A., Brozzetti, G., Pomposo, G., Lavecchia, G., Di Naccio, D., Ferrarini, F., 2010. Coseismic ground deformation of the 6 April 2009 L'Aquila earthquake (central Italy, Mw 6.3). Geophys. Res. Lett. 37, 1–6.

Bosi, C., Galadini, F., Messina, P., 1993. Neotectonic significance of bedrock fault scarps: case studies from the Lazio–Abruzzi Apennines (central Italy). Z. Geomorphol. Suppl. 94, 187–206.

Bristow, C., Jewell, C.J., 2004. GPR studies in the Piano di Pezza area of the Ovindoli–Pezza fault, Central Apennines, Italy: extending paleoseismic trench investigations with high resolution GPR profiling. Ground Penetrating Radar. Proceedings of the Tenth International Conference on Ground Penetrating Radar, pp. 555–558.

Carcaillet, J., Manighetti, I., Chauvel, C., Schlagenhauf, A., Nicole, J.M., 2008. Identifying past earthquakes on an active normal fault (Magnola, Italy) from the chemical analysis of its exhumed carbonate fault plane. Earth Planet. Sci. Lett. 271, 145–158.

Conyers, L.B., Goodman, D., 1997. Ground Penetrating Radar: An Introduction for ArchaeologistsAltaMira Press (Sage Publications), California.

Cowie, P.A., Whittaker, A.C., Attal, M., Roberts, G.P., Tucker, G.E., Ganas, A., 2008. New constraints on sediment flux dependent river incision: implications for extracting tectonic signals from river profiles. Geology 36 (7), 535–538.

Cowie, P.A., Roberts, G.P., Bull, J., Visini, F., 2012. Relationships between fault geometry, slip rate variability and earthquake recurrence in extensional settings. Geophys. J. Int. 189, 143–160.

D'Agostino, N., Giuliani, R., Mattone, M., Bonci, L., 2001. Active crustal extension in the central Apennines (Italy) inferred from GPS measurements in the interval 1994–1999. Geophys. Res. Lett. 28 (10), 2121–2124.

D'Agostino, N., Mantenuto, S., D'Anastasio, E., Giuliani, R., Mattone, M., Calcaterra, S., Gambino, P., Bonci, L., 2011. Evidence for localized active extension in the central Apennines (Italy) from global positioning system observations. Geology 39 (4), 291–294.

Faure Walker, J.P., Roberts, G.P., Cowie, P.A., Papanikolaou, I.D., Sammonds, P.R., Michetti, A.M., Phillips, R.J., 2009. Horizontal strain rates and throw rates across breached relay zones, central Italy: implications for the preservation of throw deficits at points of normal fault linkage. J. Struct. Geol. 31, 1145–1160.

Faure Walker, J.P., Roberts, G.P., Sammonds, P., Cowie, P.A., 2010. Comparison of earthquakes strains over 102 and 104 year timescales: insights into variability in the seismic cycle in the central Apennines, Italy. J. Geophys. Res. Solid Earth 115 (B10) (1978–2012).

Faure Walker, J.P., Roberts, G.P., Cowie, P.A., Papanikolaou, I., Michetti, A.M., Sammonds, Wilkinson, M., McCaffrey, K.J.W.P., Phillips, R., 2012. Relationship between topography and strain-rate in the actively-extending Italian Apennines. Earth Planet. Sci. Lett. 325, 76–84.

Galadini, F., 1999. Pleistocene changes in the central Apennine fault kinematics: a key to decipher active tectonics in central Italy. Tectonics 18, 877–894.

Galadini, F., Galli, P., 2000. Active tectonics in the central Apennines (Italy) — input data for seismic hazard assessment. Nat. Hazards 22, 225–270.

Galadini, F., Messina, P., 2001. Plio-Quaternary changes of the normal fault architecture in the central Apennines (Italy). Geodin. Acta 14, 321–344.

Galli, P., Galadini, F., Pantosti, D., 2008. Twenty years of paleoseismology in Italy. Earth-Sci. Rev. 88, 89–117.

Giaccio, B., Galadini, F., Sposato, A., Messina, P.M., Moro, M., Zreda, M., Cittadini, A., Salvi, S., Todero, A., 2002. Image processing and roughness analysis of exposed bedrock fault planes as a tool for paleoseismological analysis: results from the Campo Felice fault (central Apennines, Italy). Geomorphology 49, 281–301.

Guerrieri, L., Pascarella, F., Silvestri, S., Serva, L., 2002. Evoluzione recente dea paesaggio e dissesto geologico-idraulico: primo risultati in un'area campione dell'Appennino Centrale (valle del Salto – Rieti). Boll. Soc. Geol. Ital. 57, 453–461.

Jol, H.M., Bristow, C.S., 2003. GPR in Sediments: Advice on Data Collection, Basic Processing and Interpretation, a Good Practice Guide. Geol. Soc. Lond. Spec. Publ. 211, 9–27.

Kim, H., Arrowsmith, J.R., Crosby, C.J., Jaeger-Frank, E., Nandigam, V., Memon, A., Conner, J., Badden, S.B., Baru, C., 2006. An efficient implementation of a local binning algorithm for digital elevation model generation of LiDAR/ALSM dataset. AGU Fall Meeting Abstracts. , 1, p. 0921.

Mallet, J.L., 1992. GOCAD: a computer aided design program for geological applications. In: Turner, A.K. (Ed.), Three Dimensional Modelling With Geoscientific Information Systems. , 354. Springer, Netherlands, pp. 123–141.

Michetti, A.M., Brunamonte, F., Serva, L., Vittori, E., 1996. Trench investigations of the 1915 Fucino earthquake fault scarps (Abruzzo, Central Italy): geological evidence of large historical events. J. Geophys. Res. 101, 5921–5936.

Michetti, A.M., Audemard, F.A., Marco, S., 2005. Future trends in paleoseismology: integrated study of the seismic landscape as a vital tool in seismic hazard analyses. Tectonophysics 408, 3–21.

Morewood, N.C., Roberts, G.P., 2000. The geometry, kinematics and rates of deformation within an en echelon normal fault segment boundary, central Italy. J. Struct. Geol. 22, 1027–1047.

Neal, A., 2004. Ground-penetrating radar and its use in sedimentology: principles, problems and progress. Earth Sci. Rev. 66, 261–330.

Olhoeft, G.R., 1998. Electrical, magnetic and geometric properties that determine ground penetrating radar performance. Proc. of GPR'98, Seventh Int'l. Conf. on Ground Penetrating Radar, May 27–30, 1998. The University of Kansas, Lawrence, KS, USA, pp. 177–182.

Palumbo, L., Benedetti, L., Bourle, D., Cinque, A., Finkel, R., 2004. Slip history of the Magnola fault (Apennines, Central Italy) from ^{36}Cl surface exposure dating: evidence for strong earthquakes over the Holocene. Earth Planet. Sci. Lett. 225, 163–176.

Pantosti, D., D'Addezio, G., Cinti, F.R., 2003. Paleoseismological evidence of repeated large earthquakes along the 1980 Irpinia earthquake fault. Ann. Geofis. 36, 321–330.

Papanikolaou, I.D., Roberts, G.P., Michetti, A.M., 2005. Fault scarps and deformation rates in Lazio Abruzzo, Central Italy: comparison between geological fault slip-rate and GPS data. Tectonophysics 408, 147–176.

Patacca, E., Sartori, R., Scandone, P., 1990. Tyrrhenian basin and Apenninic arcs: kinematic relations since late Tortonian times. Mem. Soc. Geol. Ital. 45, 425–451.

Piccardi, L., Gaudemer, Y., Tapponnier, P., Boccaletti, M., 1999. Active oblique extension in the central Apennines (Italy): evidence from the Fucino region. Geophys. J. Int. 139, 499–530.

Reicherter, K., Hoffmann, N., Lindhorst, K., Krastel, S., Fernández-Steeger, T., Grützner, C., Wiatr, T., 2011. Active basins and neotectonics: morphotectonics of the Lake Ohrid Basin (FYROM and Albania). Z. Dtsch. Ges. Geowiss. 162 (2), 217–234.

Reynolds, J.M., 1997. Ground Penetrating Radar. An Introduction to Applied and Environmental Geophysics. , 1. John Wiley, Chichester 681–749.

Roberts, G.P., 2006. Multi-seismic cycle velocity and strain fields for an active normal fault system, central Italy. Earth Planet. Sci. Lett. 252, 44–51.

Roberts, G.P., Michetti, A.M., 2004. Spatial and temporal variations in growth rates along active normal fault systems: an example from Lazio–Abruzzo Apennines. J. Struct. Geol. 26, 339–376.

Roberts, G.P., Cowie, P., Papanikolaou, I., Michetti, A.M., 2004. Fault scaling relationships, deformation rates and seismic hazards: an example from Lazio–Abruzzo region, central Italy. J. Struct. Geol. 26, 377–398.

Roberts, G.P., Raithatha, B., Sileo, G., Pizzi, A., Pucci, S., Walker, J.F., Wilkinson, M., 2010. Shallow subsurface structure of the 2009 April 6 Mw 6.3 L'Aquila earthquake surface rupture at Paganica, investigated with ground-penetrating radar. Geophys. J. Int. 183, 774–790.

Rosser, N.J., Petley, D.N., Lim, M., Dunning, S.A., Allison, R.J., 2005. Terrestrial laser scanning for monitoring the process of hard rock coastal cliff erosion. Q. J. Eng. Geol. Hydrogeol. 38, 363–375.

Salvi, S., Cinti, F.R., Colini, L., D'Addezzio, G., Doumaz, F., Pettinelli, E., 2003. Investigation of the active Celano–L'Aquila fault system, Abruzzi (central Apennines, Italy) with combined ground-penetrating radar and paleoseismic trenching. Geophys. J. Int. 155, 805–818.

Schlagenhauf, A., 2009. Identification des forts seismes passes sur les failles normales actives de la region Lazio–Abruzzo (Italie centrale) par "datations cosmogeniques" (^{36}Cl) de leurs escarpments. These, Docteur de l'Universite Joseph Fourier, Grenoble, France .

Schlagenhauf, A., Gaudemer, Y., Benedetti, L., Manighetti, I., Palumbo, L., Schimmelpfennig, Finkel, R., Pou, K., 2010. Using in situ Chlorine-36 cosmonuclide to recover past earthquake histories on limestone normal fault scarps: a reappraisal of methodology and interpretations. Geophys. J. Int. 182, 36–72.

Schlagenhauf, A., Manighetti, I., Benedetti, L., Gaudemer, Y., Finkel, R., Malavieille, J., Pou, K., 2011. Earthquake supercycles in central Italy, inferred from ^{36}Cl exposure dating. Earth Planet. Sci. Lett. 307, 487–500.

Schrott, L., Sass, O., 2008. Application of field geophysics in geomorphology: advances and limitations exemplified by case studies. Geomorphology 93, 55–73.

Serpelloni, E., Anzidei, M., Baldi, P., Casula, G., Galvani, A., 2005. Crustal velocity and strain-rate fields in Italy and surrounding regions: new results from the analysis of permanent and non-permanent GPS networks. Geophys. J. Int. 161, 861–880.

Stewart, I.S., Hancock, P.L., 1990. What is a fault scarp? Episodes 13, 256–263.

Tucker, G.E., McCoy, S.W., Whittaker, A.C., Roberts, G.P., Lancaster, S.T., Phillips, R., 2011. Geomorphic significance of postglacial bedrock scarps on normal fault footwalls. J. Geophys. Res. Earth Surf. 116 (F1) (2003–2012).

Walters, R.J., Elliott, J.R., D'Agostino, N., England, P.C., Hunstad, I., Jackson, J.A., Parsons, B., Phillips, R.J., Roberts, G.P., 2009. The 2009 L'Aquila Earthquake (Central Italy): a source mechanism and implications for seismic hazard. Geophys. Res. Lett. 36.

Wells, D.L., Coppersmith, K.J., 1994. New empirical relationships among magnitude, rupture length, rupture width, rupture area, and surface displacement. Bull. Seismol. Soc. Am. 84 (4), 974–1002.

Westaway, R., Jackson, J., 1984. Surface faulting in the southern Italian Campania–Basilicata earthquake of 23rd November 1980. Nature 312, 436–438.

Whittaker, A.C., Cowie, P.A., Attal, M., Tucker, G.E., Roberts, G.P., 2007a. Contrasting transient and steady state rivers crossing active normal faults: new field observations from Italy. Basin Res. 19, 529–556.

Whittaker, A.C., Cowie, P.A., Attal, M., Tucker, G.E., Roberts, G.P., 2007b. Bedrock channel adjustment to tectonic forcing: implications for predicting river incision rates. Geology 35, 103–106.

Whittaker, A.C., Attal, M., Cowie, P.A., Tucker, G.E., Roberts, G.P., 2008. Decoding temporal and spatial patterns of uplift using transient river long profiles. Geomorphology 100, 506–526.

Wilkinson, M., McCaffrey, K.J.W., Roberts, G., Cowie, P.A., Phillips, R.J., Michetti, A.M., Vittori, E., Guerrieri, L., Blumetti, A.M., Bubeck, A., Yates, A., Sileo, G., 2010. Partitioned postseismic deformation associated with the 2009 Mw 6.3 L'Aquila earthquake surface rupture measured using a terrestrial laser scanner. Geophys. Res. Lett. 37.

Wilkinson, M., McCaffrey, K.J.W., Roberts, G., Cowie, P.A., Phillips, R.J., Degasperi, M., Vittori, E., Michetti, A.M., 2012. Distribution and magnitude of post-seismic deformation of the 2009 L'Aquila earthquake (M6.3) surface rupture measured using repeat terrestrial laser scanning. Geophys. J. Int. 189, 911–922.

Please cite this article as: Bubeck, A., et al., The tectonic geomorphology of bedrock scarps on active normal faults in the Italian Apennines mapped using combined ground penetrating..., Geomorphology (2014), http://dx.doi.org/10.1016/j.geomorph.2014.03.011